JACS ARTICLES

Published on Web 12/07/2010

Alanine Methyl Groups as NMR Probes of Molecular Structure and Dynamics in High-Molecular-Weight Proteins

Raquel Godoy-Ruiz, Chenyun Guo, and Vitali Tugarinov*

Department of Chemistry and Biochemistry, University of Maryland, College Park, Maryland 20742, United States

Received September 16, 2010; E-mail: vitali@umd.edu

Abstract: The importance and utility of Ala$^{\beta}$ methyl groups as NMR probes of molecular structure and dynamics in high-molecular-weight proteins is explored. Using ^{2}H and ^{13}C relaxation measurements in {U-^{2}H; Ala$^{\beta}$-[^{13}CHD$_2$]}-labeled Malate Synthase G (MSG)—an 82-kDa monomeric enzyme that contains 73 Ala$^{\beta}$ methyl groups—we show that the vast majority of selectively labeled Ala$^{\beta}$ methyls are highly ordered. A number of NMR applications used for solution studies of structure and dynamics of large protein molecules can benefit from proximity of Ala$^{\beta}$ methyls to the protein backbone and their high degree of ordering. In the case of MSG, these applications include the measurement of ^{1}H−^{13}C residual dipolar couplings in Ala$^{\beta}$ methyls, characterization of slow (μs-to-ms) dynamics at the substrates' binding sites, and methyl-TROSY-based NOE spectroscopy performed on {U-^{2}H; Ala$^{\beta}$-[^{13}CH$_3$]; Ile$^{\delta 1}$-[^{13}CH$_3$]; Leu,Val-[^{13}CH$_3$/^{12}CD$_3$]}-labeled samples where the number of methyl probes for derivation of distance restraints is maximized compared to the state-of-the-art ILV labeling methodology.

Introduction

Novel techniques for isotope labeling of protein samples are intimately related to methodological advances in NMR of proteins. The synergy of isotope labeling and experimental NMR methodology drives the search for optimal labeling strategies aimed at facilitating solution studies of structure and dynamics of large protein assemblies.[1,2] The labeling strategies adopted for NMR studies of large proteins usually differ from those used in analyses of smaller molecules (<∼40 kDa). While in structural NMR studies of small proteins as many proton chemical shifts as possible are assigned and subsequently NOEs connecting large numbers of sites are translated into semiquantitative distance restraints used to obtain an ensemble of structures,[3] in the case of proteins exceeding ∼50 kDa this approach becomes unproductive because spectral overlap and sensitivity limitations preclude a detailed analysis of all (protonated) positions.[4−6] Therefore, some 'key' sites in a protein are usually identified and *selectively* labeled and protonated on the otherwise deuterated background.[4,6−9] For many systems, such selective isotope enrichment provides a sufficient number of restraints to define a backbone global fold[10] and/or characterize motional properties of a large protein.[11−13] In conjunction with transverse relaxation optimized spectroscopy (TROSY) methodology,[14−19] selective isotope labeling techniques have significantly increased the size of macromolecules amenable to detailed NMR characterization.[20]

The state-of-the-art selective isotope labeling schemes employed for NMR investigations of very large proteins utilize selective incorporation of protons and ^{13}C into methyl groups of Ile (δ1 position only), Leu, and Val side chains in a highly deuterated environment (commonly known as 'ILV' labeling)[4,6,9,20,21] providing a large number of high-quality probes for NMR studies of protein structure and dynamics. Robust ILV labeling methods[9,21,22] and strategic location of ILV side chains in the hydrophobic cores of protein structures have turned ILV labeling into an

(1) Tugarinov, V.; Hwang, P. M.; Kay, L. E. *Annu. Rev. Biochem.* **2004**, *73*, 107.
(2) Sprangers, R.; Velyvis, A.; Kay, L. E. *Nat. Methods* **2007**, *4*, 697.
(3) Wüthrich, K. *NMR of Proteins and Nucleic Acids*; John Wiley & Sons: New York, 1986.
(4) Gardner, K. H.; Rosen, M. K.; Kay, L. E. *Biochemistry* **1997**, *36*, 1389.
(5) Rosen, M. K.; Gardner, K. H.; Willis, R. C.; Parris, W. E.; Pawson, T.; Kay, L. E. *J. Mol. Biol.* **1996**, *263*, 627.
(6) Tugarinov, V.; Kay, L. E. *ChemBioChem* **2005**, *6*, 1567.
(7) Gardner, K. H.; Kay, L. E. *J. Am. Chem. Soc.* **1997**, *119*, 7599.
(8) Gardner, K. H.; Kay, L. E. *Annu. Rev. Biophys. Biomol. Struct.* **1998**, *27*, 357.
(9) Goto, N. K.; Gardner, K. H.; Mueller, G. A.; Willis, R. C.; Kay, L. E. *J. Biomol. NMR* **1999**, *13*, 369.
(10) Tugarinov, V.; Choy, W. Y.; Orekhov, V. Y.; Kay, L. E. *Proc. Natl. Acad. Sci. U.S.A.* **2005**, *102*, 622.
(11) Sprangers, R.; Kay, L. E. *Nature* **2007**, *445*, 618.
(12) Velyvis, A.; Yang, Y. R.; Schachman, H. K.; Kay, L. E. *Proc. Natl. Acad. Sci. U.S.A.* **2007**, *104*, 8815.
(13) Religa, T. L.; Sprangers, R.; Kay, L. E. *Science* **2010**, *328*, 98.
(14) Pervushin, K.; Riek, R.; Wider, G.; Wüthrich, K. *Proc. Natl. Acad. Sci. U.S.A.* **1997**, *94*, 12366.
(15) Pervushin, K.; Riek, R.; Wider, G.; Wüthrich, K. *J. Am. Chem. Soc.* **1998**, *120*, 6394.
(16) Miclet, E.; Williams Jr, D. C.; Clore, G. M.; Bryce, D. L.; Boisbouvier, J.; Bax, A. *J. Am. Chem. Soc.* **2004**, *126*, 10560.
(17) Tugarinov, V.; Hwang, P. M.; Ollerenshaw, J. E.; Kay, L. E. *J. Am. Chem. Soc.* **2003**, *125*, 10420.
(18) Tugarinov, V.; Sprangers, R.; Kay, L. E. *J. Am. Chem. Soc.* **2004**, *126*, 4921.
(19) Tugarinov, V.; Ollerenshaw, J. E.; Kay, L. E. *J. Am. Chem. Soc.* **2005**, *127*, 8214.
(20) Ruschak, A. M.; Kay, L. E. *J. Biomol. NMR* **2010**, *46*, 75.
(21) Tugarinov, V.; Kay, L. E. *J. Biomol. NMR* **2004**, *28*, 165.
(22) Gans, P.; Hamelin, O.; Sounier, R.; Ayala, I.; Durá, M. A.; Amero, C. D.; Noirclerc-Savoye, M.; Franzetti, B.; Plevin, M. J. J. B. *Angew. Chem., Int. Ed.* **2010**, *49*, 1958.

10.1021/ja1083656

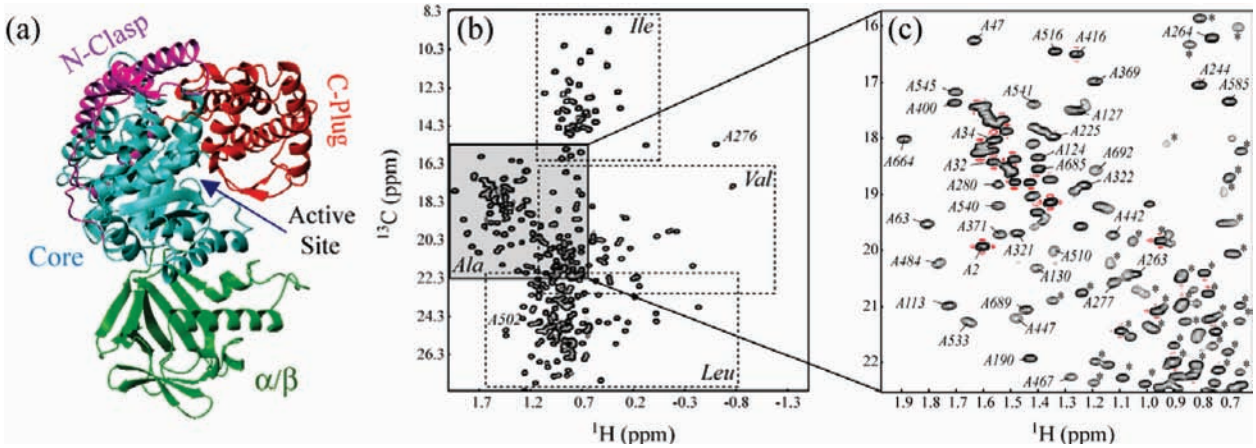

Figure 1. (a) Molecular organization of Malate Synthase G. The four domains of the protein are shown with different colors. The figure was prepared using the program Molmol.[70] (b) Methyl ^{1}H−^{13}C HMQC[17,68,69] correlation map recorded on a 0.7 mM {Ala$^{\beta}$-[^{13}CH$_3$]; Ile$^{\delta1}$-[^{13}CH$_3$]; Leu,Val-[^{13}CH$_3$/^{12}CD$_3$]}-labeled MSG (37 °C, 600 MHz). The regions of the map approximately corresponding to Ile$^{\delta1}$, Val$^{\gamma}$, and Leu$^{\delta}$ methyl positions are enclosed in dashed rectangles. The region enclosed in a solid rectangle and highlighted corresponds to Ala$^{\beta}$ methyls. (c) The Ala$^{\beta}$ part of the map 'zoomed' from the region highlighted in (b). Cross-peaks arising from Val$^{\gamma}$ and Leu$^{\delta}$ correlations are marked with asterisks. Ala$^{\beta}$ assignments are indicated for selected methyls from refs 29, 30.

indispensable tool for NMR studies of large proteins and macromolecular complexes. Selective ^{13}CH$_3$ labeling of ILV positions in large proteins on a deuterated background coupled with methyl-TROSY[17] techniques have had a significant impact on NMR studies of structure and dynamics of large protein assemblies up to ~800 kDa in molecular weight.[2,10,11,13,23−25]

The availability of only three ILV probes represents a serious limitation for structural and dynamics studies of large proteins. Methyl groups of alanines can serve as an attractive extension of the ILV labeling methodology. Ala methyls are located in close proximity to the backbone; their flexibility is therefore reduced compared to other methyl-bearing side chains in proteins. Ala is one of the most frequently encountered residues in protein hydrophobic cores and at molecular interfaces.[26] Recently, several reports have focused upon extending the ILV methodology with (selective) labeling of Ala$^{\beta}$ methyl positions in large proteins.[27−30] Isaacson et al. have introduced a labeling strategy for selective incorporation of ^{13}CH$_3$ groups into alanine residues on a deuterated background.[27] Specific protonation of Ala methyls to a level of 95% with minimal background labeling has been reported.[28] One of the most promising aspects of the Ala labeling approaches is the possibility of concomitant labeling of ILV methyl positions in the same protein sample.[27] Here, we demonstrate in detail the utility of Ala methyl groups as probes of structure and dynamics in high-molecular-weight proteins on the example of an 82-kDa monomeric enzyme Malate Synthase G (MSG, 723-residues) using both selective ^{13}CHD$_2$ labeling of Ala$^{\beta}$ methyls as well as the ^{13}CH$_3$ labeling of ILV methyl positions supplemented with ^{13}CH$_3$ labeling of Ala$^{\beta}$ sites. Alanine is the most abundant amino acid in MSG constituting 10.1% of total amino acid content (73 residues) serving as an excellent probe of structural and dynamical properties of the molecule.

MSG has been characterized in considerable detail by multidimensional NMR methods in the past decade.[10,31−33] MSG is one of the two enzymes of the 'glyoxylate shunt', a biochemical bypass used by microorganisms for biosynthesis under anaerobic conditions.[34] It catalyzes the Claisen condensation of glyoxylate and Acetyl-CoA to produce malate. The X-ray structure of MSG in complex with its substrate glyoxylate has been solved at 2.0 Å resolution by Remington and co-workers.[35] Later, the 1.95 Å resolution X-ray structure of the ternary abortive complex of MSG with pyruvate (glyoxylate mimic) and acetyl-CoA has been reported by the same group,[36] showing that the enzyme adopts essentially the same structure as in the complex with glyoxylate. The global fold of the apo-form of MSG has been determined from NMR data exclusively using selective methyl labeling techniques[10] and subsequently refined via a combined SAXS/NMR protocol.[37] MSG is composed of four domains color-coded in Figure 1a: (i) a centrally located molecular core based on a stable β8/α8 barrel fold, (ii) an N-terminal α-helical clasp, (iii) an α/β domain appended to the molecular core, and (iv) a C-terminal end of the enzyme consisting of a five-helix plug connected to the barrel by a flexible loop. The active site of the enzyme is located in a cleft

(23) Gelis, I.; Bonvin, A. M.; Keramisanou, D.; Koukaki, M.; Gouridis, G.; Karamanou, S.; Economou, A.; Kalodimos, C. G. *Cell* **2007**, *131*, 756.
(24) Amero, C.; Schanda, P.; Durá, M. A.; Ayala, I.; Marion, D.; Franzetti, B.; Brutscher, B.; Boisbouvier, J. *J. Am. Chem. Soc.* **2009**, *131*, 3448.
(25) Hamel, D. J.; Dahlquist, F. W. *J. Am. Chem. Soc.* **2005**, *127*, 9676.
(26) Fernandez, A.; Scott, L. R.; Scheraga, H. A. *J. Phys. Chem.* **2003**, *107*, 9929.
(27) Isaacson, R. L.; Simpson, P. J.; Liu, M.; Cota, E.; Zhang, X.; Freemont, P.; Matthews, S. *J. Am. Chem. Soc.* **2007**, *129*, 15428.
(28) Ayala, I.; Sounier, R.; Usé, N.; Gans, P.; Boisbouvier, J. *J. Biomol. NMR* **2009**, *43*, 111.
(29) Sheppard, D.; Guo, C.; Tugarinov, V. *J. Am. Chem. Soc.* **2009**, *131*, 1364.
(30) Sheppard, D.; Guo, C.; Tugarinov, V. *J. Biomol. NMR* **2009**, *43*, 229.
(31) Tugarinov, V.; Muhandiram, R.; Ayed, A.; Kay, L. E. *J. Am. Chem. Soc.* **2002**, *124*, 10025.
(32) Tugarinov, V.; Kay, L. E. *J. Mol. Biol.* **2003**, *327*, 1121.
(33) Sheppard, D.; Sprangers, R.; Tugarinov, V. *Prog. Nucl. Magn. Reson. Spectrosc.* **2010**, *56*, 1.
(34) Kronberg, H. L.; Krebs, H. A. *Nature* **1957**, *179*, 988.
(35) Howard, B. R.; Endrizzi, J. A.; Remington, S. J. *Biochemistry* **2000**, *39*, 3156.
(36) Anström, D. M.; Kallio, K.; Remington, S. J. *Protein Sci.* **2003**, *12*, 1822.
(37) Grishaev, A.; Tugarinov, V.; Trewhella, J.; Kay, L. E.; Bax, A. *J. Biomol. NMR.* **2008**, *40*, 95.
(38) Ishima, R.; Petkova, A. P.; Louis, J. M.; Torchia, D. A. *J. Am. Chem. Soc.* **2001**, *123*, 6164.
(39) Tugarinov, V.; Kay, L. E. *Biochemistry* **2005**, *44*, 15970.
(40) Ishima, R.; Louis, J. M.; Torchia, D. A. *J. Am. Chem. Soc.* **1999**, *121*, 11589.

at the interface between the C-terminal plug and the loops at the C-termini of the core barrel β-strands[32,35] (Figure 1a).

Materials and Methods

NMR Samples. Two NMR samples of MSG have been used in this work: (i) {U-[^{15}N,^{2}H]; Ala$^{\beta}$-[^{13}CHD$_2$]}-labeled sample, (ii) {U-[^{15}N,^{2}H]; Ala$^{\beta}$-[^{13}CH$_3$]; Ile$^{\delta1}$-[^{13}CH$_3$]; Leu,Val-[^{13}CH$_3$/^{12}CD$_3$]}-labeled sample. Both samples were prepared using [U-^{2}H]-D-glucose as the main carbon source, and ^{15}N-ammonium chloride as the main source of nitrogen. Selective labeling of Ala$^{\beta}$ positions with ^{13}CHD$_2$ groups (the {U-[^{15}N,^{2}H]; Ala$^{\beta}$-[^{13}CHD$_2$]}-labeled sample) has been achieved following the protocol of Ayala et al.[28] by addition of (i) 700 mg of {2,3,3-d_3, 3-^{13}C$_1$}-L-alanine (methyl-^{13}CHD$_2$-alanine), (ii) 2.5 g of succinate-d_4, (iii) 200 mg for α-keto-isovalerate-d_7, and (iv) 60 mg of L-isoleucine-d_{10} to 1 L of D$_2$O-based M9 medium 1 h prior to induction of protein overexpression with 1 mM IPTG. Selective ^{13}CH$_3$ labeling of all ILV positions together with Ala$^{\beta}$ methyls ({U-[^{15}N,^{2}H]; Ala$^{\beta}$-[^{13}CH$_3$]; Ile$^{\delta1}$-[^{13}CH$_3$]; Leu,Val-[^{13}CH$_3$/^{12}CD$_3$]}-labeled sample) has been achieved by addition of (i) 700 mg of {2-d_1,3-^{13}C$_1$}-L-alanine; (ii) 2.5 g of succinate-d_4; (iii) 120 mg of 2-keto-3-d_1-methyl-d_3-4-^{13}C-butyrate ([U-^{2}H; methyl-^{13}CH$_3$/^{12}CD$_3$]-α-keto-isovalerate); and (iv) 60 mg of 2-keto-3-d_2-4-^{13}C-butyrate ([U-^{2}H; methyl-^{13}CH$_3$]-α-ketobutyrate) to 1 L of the medium 1 h prior to induction. Both {3,3-d_2, 3-^{13}C$_1$}- and {3-^{13}C$_1$}-L-alanine were obtained from Isotec/Sigma-Aldrich (Miamisburg, OH) and deuterated at α-position using the protocol described previously.[27] All the other chemicals and biosynthetic precursors have been obtained from CIL (Andover, MA) except for the deuterated salt of α-keto-isovaleric acid (α-keto-isovalerate-d_7) which has been purchased from CDN Isotopes (Quebec, Canada). {Ala$^{\beta}$-[^{13}CHD$_2$]}- and {Ala$^{\beta}$-[^{13}CH$_3$]; Ile$^{\delta1}$-[^{13}CH$_3$]; Leu,Val-[^{13}CH$_3$/^{12}CD$_3$]}-labeled samples of MSG were 0.7 mM and 1.0 mM in protein concentration, respectively, in 99% D$_2$O and contained 25 mM sodium phosphate buffer (pH 7.1, uncorrected), 20 mM MgCl$_2$, 5 mM DTT, and 0.05% NaN$_3$.

NMR Spectroscopy. All NMR measurements were performed at 37 °C on a Bruker Avance III 600 MHz spectrometer equipped with a room temperature probe. Complete assignments of Ala$^{\beta}$ methyls have been obtained earlier using methyl 'out-and-back' experiments and a [U-^{13}C]-Pyruvate-derived sample of MSG.[29,30] Availability of both ^{13}C and ^{2}H nuclei in the same ^{13}CHD$_2$ methyl isotopomer allows one to measure both ^{2}H and ^{13}C relaxation on a single protein sample.[33,38,39] $R_{1\rho}$ and R_1 relaxation rates of ^{13}C spins in ^{13}CHD$_2$ Ala$^{\beta}$ methyl groups have been measured on {Ala$^{\beta}$-[^{13}CHD$_2$]}-MSG using the acquisition parameters and pulse schemes provided in the Supporting Information of Tugarinov and Kay.[39] These experiments are very similar to those used by Torchia and co-workers in ^{13}C relaxation studies of HIV-1 protease.[38,40] ^{13}C $R_{1\rho}$ experiments have been recorded with two spin-lock field strengths: 1.2 and 2.0 kHz.

It has been shown earlier that the choice of appropriate transverse, M_+(CHD$_2$),[6,19,33] and longitudinal, M_L(CHD$_2$),[33,41] ^{2}H magnetization modes that decay nearly single-exponentially[19,41] allows the recording and interpretation of ^{2}H relaxation rates in ^{13}CHD$_2$ methyl isotopomers of large proteins in much the same manner as this is accomplished in simpler, single-deuteron ^{13}CH$_2$D spin-systems.[19,42] These ^{2}H magnetization terms are given by: $M_+(\mathrm{CHD_2}) = -[C_z(D_{y,1} + D_{y,2})]\{\sin(4\pi J_{\mathrm{CD}}T_C)\} - [C_z(D_{y,1}{}^2D_{y,2} + D_{y,1}D_{y,2}{}^2)]\{(1/2)\sin(8\pi J_{\mathrm{CD}}T_C) - \sin(4\pi J_{\mathrm{CD}}T_C)\}$, and $M_L(\mathrm{CHD_2}) = C_z\{D_{z,1} + D_{z,2} - (3/2)(D_{z,1}D^2_{z,2} + D_{z,2}D^2_{z,1})\}$ where A_i is a Cartesian spin operator of nucleus i ($i = x,y,z$), J_{CD} is the ^{13}C−^{2}H scalar coupling in a methyl group (~20 Hz), T_C is the delay used for evolution of J_{CD}, and the subscripts 1,2 are used to distinguish the two deuterons of the ^{13}CHD$_2$ spin-system. ^{2}H relaxation measurements in Ala$^{\beta}$ ^{13}CHD$_2$ methyl isotopomers were performed using the schemes of Figure 6 of Tugarinov et al.[19] for $R_2[M_+(\mathrm{CHD_2})]$ rates and Figure 1a of Tugarinov and Kay[41] for $R_1[M_L(\mathrm{CHD_2})]$ rates. ^{2}H $R_2[M_+(\mathrm{CHD_2})]$, $R_1[M_L(\mathrm{CHD_2})]$, and ^{13}C $R_{1\rho}$,R_1 rates have been obtained by fitting the peak intensity decays to single-exponential functions $A\exp(-RT)$ where R is the relaxation rate and T is the parametrically varied relaxation delay. The uncertainties in ^{2}H and ^{13}C relaxation rates have been estimated from duplicate measurements or from the noise-floor in the spectra whichever was the highest.

Methyl-TROSY-based multiple quantum (MQ) CPMG[43,44] experiments for quantification of methyl dynamics on the micro-to-millisecond time scale have been recorded and analyzed as described previously[45] using the {Ala$^{\beta}$-[^{13}CH$_3$]; Ile$^{\delta1}$-[^{13}CH$_3$]; Leu,Val-[^{13}CH$_3$/^{12}CD$_3$]}-labeled sample. The CPMG[43,44] frequency ν_{CPMG} spanned the range between 0 and 1.1 kHz, while the ^{13}C carrier has been placed at 19 ppm, the center of the Ala$^{\beta}$ methyl region. Transverse relaxation violated coherence transfer ('forbidden') relaxation series for quantification of the amplitudes of ^{13}CH$_3$−Ala$^{\beta}$ methyl axis motions on the pico-to-nanosecond time scale have been acquired and analyzed as described elsewhere.[33,46] Methyl ^{1}H−^{13}C residual dipolar coupling (RDC) have been measured from the F_1(^{13}C) dimension of ^{1}H−^{13}C IPAP-HSQC spectra[47,48] recorded on the {Ala$^{\beta}$-[^{13}CHD$_2$]}-labeled MSG (see Results and Discussion for details). Weak alignment of MSG has been achieved by addition of pf1 phage particles[49] to the final concentration of ~12 mg/mL (D$_2$O splitting 9.8 Hz). ^{1}H−^{13}C 3D HMQC-NOESY[50] and 3D HMQC-NOESY-HMQC[51] spectra have been recorded on the {Ala$^{\beta}$-[^{13}CH$_3$]; Ile$^{\delta1}$-[^{13}CH$_3$]; Leu,Val-[^{13}CH$_3$/^{12}CD$_3$]}-labeled sample using three-dimensional adaptations of the previously published methyl-TROSY-based 4D HMQC-NOESY-HMQC scheme.[52−54] Uniform sampling was used in all indirect dimensions. NOE mixing period of 175 ms was used in all NOESY experiments.[52] ^{1}H−^{13}C MQ relaxation rates of Ala$^{\beta}$ ^{13}CH$_3$ methyls have been measured as described previously.[21] NMR spectra have been processed and analyzed using NMRDraw/NMRPipe and associated software.[55] NOE data have been analyzed using tcl/tk scripts written in-house for the program NMRView.[56]

^{2}H and ^{13}C Relaxation Data Analysis in Alaβ ^{13}CHD$_2$ Groups. ^{2}H and ^{13}C relaxation rates are related to molecular dynamics through their dependence on a linear combination of the motional power spectra (spectral density functions, J) at a finite number of frequencies. The simplest model-free[57,58] form of the spectral density applicable to methyl group dynamics has been used throughout this work,[59−61]

(41) Tugarinov, V.; Kay, L. E. *J. Am. Chem. Soc.* **2006**, *128*, 12484.
(42) Muhandiram, D. R.; Yamazaki, T.; Sykes, B. D.; Kay, L. E. *J. Am. Chem. Soc.* **1995**, *117*, 11536.
(43) Carr, H. Y.; Purcell, E. M. *Phys. Rev.* **1954**, *94*, 630.
(44) Meiboom, S.; Gill, D. *Rev. Sci. Instrum.* **1958**, *29*, 688.
(45) Korzhnev, D. M.; Kloiber, K.; Kanelis, V.; Tugarinov, V.; Kay, L. E. *J. Am. Chem. Soc.* **2004**, *126*, 3964.
(46) Tugarinov, V.; Sprangers, R.; Kay, L. E. *J. Am. Chem. Soc.* **2007**, *129*, 1743.
(47) Yang, D.; Nagayama, K. *J. Magn. Reson., Ser. A* **1996**, *118*, 117.
(48) Ottiger, M.; Delaglio, F.; Bax, A. *J. Magn. Reson.* **1998**, *131*, 373.
(49) Hansen, M. R.; Mueller, L.; Pardi, A. *Nat. Struct. Biol.* **1998**, *5*, 1065.
(50) Fesik, S. W.; Zuiderweg, E. R. P. *J. Magn. Reson.* **1988**, *78*, 588.
(51) Clore, G. M.; Gronenborn, A. M. *Annu. Rev. Biophys. Chem.* **1991**, *20*, 29.
(52) Tugarinov, V.; Kay, L. E.; Ibraghimov, I.; Orekhov, V. Y. *J. Am. Chem. Soc.* **2005**, *127*, 2767.
(53) Clore, G. M.; Kay, L. E.; Bax, A.; Gronenborn, A. M. *Biochemistry* **1991**, *30*, 12.
(54) Vuister, G. W.; Clore, G. M.; Gronenborn, A. M.; Powers, R.; Garrett, D. S.; Tschudin, R.; Bax, A. *J. Magn. Reson., Ser. B* **1993**, *101*, 210.
(55) Delaglio, F.; Grzesiek, S.; Vuister, G. W.; Zhu, G.; Pfeifer, J.; Bax, A. *J. Biomol. NMR* **1995**, *6*, 277.
(56) Johnson, B. A.; Blevins, R. A. *J. Biomol. NMR* **1994**, *4*, 603.
(57) Lipari, G.; Szabo, A. *J. Am. Chem. Soc.* **1982**, *104*, 4546.
(58) Lipari, G.; Szabo, A. *J. Am. Chem. Soc.* **1982**, *104*, 4559.
(59) Kay, L. E.; Torchia, D. A. *J. Magn. Reson.* **1991**, *95*, 536.
(60) Skrynnikov, N. R.; Millet, O.; Kay, L. E. *J. Am. Chem. Soc.* **2002**, *124*, 6449.
(61) Woessner, D. E. *J. Chem. Phys.* **1962**, *37*, 647.

$$J(\omega) = a^2 S^2_{\text{axis}}\left[\frac{A_1\tau_1}{1+(\omega\tau_1)^2} + \frac{A_2\tau_2}{1+(\omega\tau_2)^2} + \frac{A_3\tau_3}{1+(\omega\tau_3)^2}\right] + (1 - a^2 S^2_{\text{axis}})\frac{\tau'}{1+(\omega\tau')^2} \quad (1)$$

where S^2_{axis} is the generalized order parameter squared describing the amplitude of motion of the methyl C_{v3}-symmetry axis (located along the $C^{\alpha}-C^{\beta}$ bond in Ala); $a = (3\cos^2(\theta) - 1)/2$, θ is the angle between the C−D bond and the methyl 3-fold symmetry axis ($a = 1/3$ was used for dipolar and quadrupolar interactions in this work corresponding to the distance r_{CH} in the methyl group equal to 1.135 Å,[39,62,63] while $a = 1$ should be used for ^{13}C chemical shift anisotropy, CSA, interaction); $A_1 = (3/4)\sin^4(\alpha)$, $A_2 = 3\sin^2(\alpha)\cos^2(\alpha)$, $A_3 = [(3/2)\cos^2(\alpha) - 0.5]^2$, $\tau_1 = (4D_{\|} + 2D_{\perp})^{-1}$, $\tau_2 = (D_{\|} + 5D_{\perp})^{-1}$, $\tau_3 = (6D_{\perp})^{-1}$, $D_{\|}$ and $D_{\perp}$ are the components of the molecular diffusion tensor, α is the angle between the methyl three-fold and the unique diffusion axis, and $1/\tau' = 1/\tau_f + 1/\tau_{c,eff}$ with $\tau_{c,eff} = (2D_{\|} + 4D_{\perp})^{-1}$ the effective correlation time of overall rotation, and τ_f the time-scale of local methyl motions. Direction cosines for the $C^{\alpha}-C^{\beta}$ three-fold axes were obtained from the X-ray coordinates of MSG (pdb code 1d8c[35]). The errors in ^{2}H and ^{13}C relaxation rates have been propagated to the errors in S^2_{axis} and τ_f via Monte Carlo simulations.[64]

The following expressions for the transverse and longitudinal ^{2}H magnetization modes have been used in analyses of ^{2}H rates,

$$R_2[M_+(\text{CHD}_2)] = (1/80)(2\pi e^2 qQ/h)^2[9J(0) + 15J(\omega_D) + 6J(2\omega_D)] \quad (2)$$

$$R_1[M_L(\text{CHD}_2)] = (3/40)(2\pi e^2 qQ/h)^2[4J(\omega_D) + 4J(2\omega_D)] \quad (3)$$

where (e^2qQ/h) is the ^{2}H quadrupolar coupling constant (167 kHz[65] used in this work) and $J(\omega)$ is the same as in eq 1. Equation 2 can be used as long as $J(0) \gg J(\omega_D)$, $J(2\omega_D)$, a condition usually satisfied in proteins with rotational correlation times in excess of ~20 ns, despite that the quadrupolar relaxation of $M_+(\text{CHD}_2)$ is not single-exponential at ω_D and $2\omega_D$ frequencies.[19] The relaxation of $M_L(\text{CHD}_2)$ is very close to single-exponential with the errors in derived τ_f values not exceeding 2.5% for proteins with $\tau_{c,eff}$ on the order of 50 ns, $\tau_f > 5$ ps and any value of S^2_{axis}.[41]

^{13}C $R_{1\rho}$ rates have been corrected for offset effects to extract ^{13}C R_2 rates.[66] ^{13}C R_2,R_1 rates were fitted to the expressions for ^{13}C relaxation in ^{13}CHD$_2$ groups described earlier by Torchia and co-workers[38] (see also eqs S3−S4 in the Supporting Information of Tugarinov and Kay[39]). Although the lines of a 1:2:3:2:1 ^{13}C(H)D$_2$ pentet relax differently, the equations used for interpretation of ^{13}C relaxation rates take this into account, albeit approximately and in the limit where $J(0) \gg J(\omega_C)$.[38,39] ^{2}H spin-flips that can interchange the components of the pentet are slower in large molecules (^{2}H T_1 on the order of 80−100 ms in ILV methyls of MSG), while the average Ala$^{\beta}$ ^{13}C T_2 is 30 ms in [Ala$^{\beta}$-^{13}CHD$_2$]-MSG. Therefore, for the relaxation delays used for ^{13}C R_2 measurements in this study (<40 ms), ^{2}H spin-flips should have practically no effect on the extracted ^{13}C relaxation rates.

Calculations performed for {Ala$^{\beta}$-[^{13}CHD$_2$]}-labeled MSG show that contributions to ^{13}C relaxation rates from dipolar interactions with external ^{2}H nuclei can be accounted for by placing a single deuteron at a uniform distance of 1.8 Å from the methyl carbon in question. Contributions from dipolar fields due to external protons in the highly deuterated {Ala$^{\beta}$-[^{13}CHD$_2$]}-labeled sample are generally very small. Nevertheless, they were taken into account on a residue-specific basis by calculating the effective distance $(\sum_{\text{ext}} \langle r^{-6}_{\text{CHext}}\rangle)^{-1/6}$ for each given Ala methyl group (distance between the methyl carbon and all external proton spins in other Alaβ ^{13}CHD$_2$ methyls) and then using this value in the course of the data fitting. The average effective distance $(\sum_{\text{ext}} \langle r^{-6}_{\text{CHext}}\rangle)^{-1/6}$ in the {Ala$^{\beta}$-[^{13}CHD$_2$]}-labeled MSG dissolved in D$_2$O is 4.5 Å assuming random protonation at the level of 3%. Note that this average distance is slightly higher than that calculated for ^{13}CHD$_2$ methyls in a {Ile$^{\delta1}$-[^{13}CHD$_2$]}-labeled MSG (4.0 Å) reflecting the fact that Ala side chains are shorter than Ile side chains and do not protrude as far into the hydrophobic core of the protein. A uniform value of 18 ppm[67] was used for Ala$^{\beta}$ ^{13}C CSA (assumed axially symmetric) with the exception of a small number of residues (see Results and Discussion).

To estimate the effective rotational correlation time of the global reorientation of MSG, $\tau_{c,eff}$, diffusion measurements on both samples of MSG have been performed as described elsewhere.[19] Earlier, analysis ^{15}N spin relaxation data of MSG provided the value of $D_{\|}/D_{\perp} = 1.21 \pm 0.03$ with the polar angles describing the orientation of the unique diffusion axis relative to the molecular inertia coordinate frame of $\theta = 13 \pm 4°$ and $\phi = 48 \pm 17°$.[19] A value of $\tau_{c,eff} = 48$ ns was obtained from diffusion measurements for the {Ala$^{\beta}$-[^{13}CH$_3$]; Ile$^{\delta1}$-[^{13}CH$_3$]; Leu,Val-[^{13}CH$_3$/^{12}CD$_3$]}-labeled MSG, while a value of 57 ns was obtained for the {Ala$^{\beta}$-[^{13}CHD$_2$]}-labeled sample using a procedure described in detail previously.[19] The difference in $\tau_{c,eff}$ values between the two samples reflects the significantly higher concentration of the {Ala$^{\beta}$-[^{13}CHD$_2$]}-labeled protein (1.0 mM vs. 0.7 mM) and the noted dependence of sample viscosity (and therefore $\tau_{c,eff}$) on protein concentration.[19]

Results and Discussion

Isotope Labeling of Ala$^{\beta}$ Methyl Positions in Large Proteins. Specific ^{13}C labeling and protonation of Ala$^{\beta}$ methyls to a level of 95% with minimal background labeling (<1%) in minimal D$_2$O-based bacterial medium supplemented with large amounts of selectively ^{13}C$^{\beta}$-labeled α-deuterated alanine and coaddition of three deuterated biochemical compounds: (i) α-ketoisovalerate-d_7, (ii) succinate-d_4, and (iii) L-isoleucine-d_{10} has been reported recently by Boisbouvier and co-workers.[28] This labeling protocol has been followed for production of {Ala$^{\beta}$-[^{13}CHD$_2$]}-MSG in this work via the use of {2,3,3-d_3, 3-^{13}C$_1$}-L-alanine. However, to increase the number of available methyl probes, it would clearly be advantageous to combine selective labeling of Ala$^{\beta}$ positions with ILV methyl labeling. The use of selectively ^{13}CH$_3$-labeled Ala ({2-d_3, 3-^{13}C$_1$}-L-alanine) in combination with (i) selectively ^{13}CH$_3$-labeled α-ketobutyrate for labeling of Ile$^{\delta1}$ positions, (ii) ^{13}CH$_3$/^{12}CD$_3$-labeled α-ketoisovalerate for labeling of Val$^{\gamma}$ and Leu$^{\delta}$ sites, and (iii) deuterated succinate, achieved exactly this purpose (see Materials and Methods). Figure 1b,c shows the ^{1}H−^{13}C methyl-TROSY (HMQC[17,68,69]) correlation map recorded on the {Ala$^{\beta}$-[^{13}CH$_3$]; Ile$^{\delta1}$-[^{13}CH$_3$]; Leu,Val-[^{13}CH$_3$/^{12}CD$_3$]}-labeled MSG. Ala$^{\beta}$ methyl signals resonate in a distinct region of the spectrum. Although the overlap of resonances within the Ala$^{\beta}$ group is very substantial, Ala$^{\beta}$ signals do not overlap with either Val$^{\gamma}$ or Leu$^{\delta}$ methyl groups (Figure 1b,c).

In full agreement with previous observations,[28] no signs of scrambling of isotope labels from alanine to other amino acids have been detected in either sample. In fact, a comparison of

(62) Ottiger, M.; Bax, A. *J. Am. Chem. Soc.* **1999**, *121*, 4690.
(63) Mittermaier, A.; Kay, L. E. *J. Biomol. NMR* **2002**, *23*, 35.
(64) Kamith, U.; Shriver, J. W. *J. Biol. Chem.* **1989**, *264*, 5586.
(65) Mittermaier, A.; Kay, L. E. *J. Am. Chem. Soc.* **1999**, *121*, 10608.
(66) Peng, J. W.; Wagner, G. *Methods Enzymol.* **1994**, *239*, 563.
(67) Ye, C.; Fu, R.; Hu, J.; Hou, L.; Ding, S. *Magn. Reson. Chem.* **1993**, *31*, 699.
(68) Mueller, L. *J. Am. Chem. Soc.* **1979**, *101*, 4481.
(69) Bax, A.; Griffey, R. H.; Hawkings, B. L. *J. Magn. Reson.* **1983**, *55*, 301.
(70) Koradi, R.; Billeter, M.; Wüthrich, K. *J. Mol. Graphics* **1996**, *14*, 51.

signal intensities of ILV methyls in the {Ala$^{\beta}$-[$^{13}CH_3$]; Ile$^{\delta1}$-[$^{13}CH_3$]; Leu,Val-[$^{13}CH_3/^{12}CD_3$]}-labeled sample with those obtained in {Ile$^{\delta1}$-[$^{13}CH_3$]; Leu,Val-[$^{13}CH_3/^{12}CD_3$]}-labeled MSG (after normalization for different sample concentrations) indicated that the level of isotope incorporation into ILV methyl positions is not significantly (to within less than ~10%) compromised by addition of large amounts of labeled Ala to the medium. This is the direct consequence of the fact that the biosynthetic pathway leading to incorporation of labels into Ile$^{\delta1}$ positions is 'short-circuited' by addition of the suitably labeled α-ketobutyrate to the medium, while the pathway leading to labeling of Val$^{\gamma}$ and Leu$^{\delta}$ sites is 'short-circuited' by addition of the α-keto-isovalerate precursor.

It might have been expected that the addition of α-ketobutyrate to the medium instead of deuterated isoleucine in order to ensure $^{13}CH_3$ labeling at Ile$^{\delta1}$ methyl positions would result in partial $^{13}CH_3$ labeling at Ile$^{\gamma2}$ methyl sites (arising from alanine-derived [3-$^{13}CH_3$]-pyruvate entering into the biosynthetic cycle of Ile instead of the completely deuterated pyruvate from [U-^{2}H]-glucose). Nevertheless, Ile$^{\gamma2}$ ^{1}H−^{13}C correlations have not been detected in the ^{1}H−^{13}C methyl-TROSY spectra recorded on the {Ala$^{\beta}$-[$^{13}CH_3$]; Ile$^{\delta1}$-[$^{13}CH_3$]; Leu,Val-[$^{13}CH_3/^{12}CD_3$]}-MSG indicating that the molecules of pyruvate originate predominantly from [U-^{2}H]-glucose during protein production.

To estimate whether the addition of Ala$^{\beta}$ protons is detrimental to the quality of methyl-TROSY spectra, we have measured methyl MQ ^{13}C−^{1}H T_2 times and ^{1}H T_1 values of Ile$^{\delta1}$ and Val$^{\gamma}$/Leu$^{\delta}$ methyls in {Ala$^{\beta}$-[$^{13}CH_3$]; Ile$^{\delta1}$-[$^{13}CH_3$]; Leu,Val-[$^{13}CH_3/^{12}CD_3$]}-MSG and {Ile$^{\delta1}$-[$^{13}CH_3$]; Leu,Val-[$^{13}CH_3/^{12}CD_3$]}-MSG. The average MQ ^{13}C−^{1}H T_2 in the Ala$^{\beta}$-[$^{13}CH_3$]-labeled sample was 43 ± 12 ms, while the value of 39 ± 11 ms was obtained in {Ile$^{\delta1}$-[$^{13}CH_3$]; Leu,Val-[$^{13}CH_3/^{12}CD_3$]}-MSG for the same subset of well resolved peaks. It is clear from this comparison that the differences in MQ ^{13}C−^{1}H T_2 values between the two labeling schemes are small and that additional protonation at Ala$^{\beta}$ sites should not significantly compromise the quality of methyl-TROSY correlation maps. Interestingly, somewhat higher average MQ ^{13}C−^{1}H T_2 values were obtained for Ala$^{\beta}$ methyls in {Ala$^{\beta}$-[$^{13}CH_3$]; Ile$^{\delta1}$-[$^{13}CH_3$]; Leu,Val-[$^{13}CH_3/^{12}CD_3$]}-MSG, 51 ± 6 ms, reflecting the fact that Ala$^{\beta}$ methyls belong to much shorter side chains than ILV methyls and do not protrude equally far into the hydrophobic core of the protein. Likewise, no significant differences were observed between ^{1}H T_1 values estimated in the two samples (0.65 ± 0.2 s and 0.62 ± 0.2 s in the samples with and without Ala$^{\beta}$-[$^{13}CH_3$] labeling, respectively).

Fast Dynamics of Ala$^{\beta}$ Methyl Groups. Whereas transverse and longitudinal ^{2}H relaxation rates in $^{13}CHD_2$ methyl groups can be interpreted in terms of microdynamic parameters of pico-to-nanosecond motions in a straightforward manner by consideration of only a single and strong ^{2}H quadrupolar interaction,[42] the interpretation of ^{13}C relaxation rates in $^{13}CHD_2$ isotopomers is generally more involved. Indeed, using an average set of motional parameters for (ordered) Ala$^{\beta}$ methyls in MSG (S^2_{axis} = 0.90; τ_f = 40 ps; ^{13}C CSA = 18 ppm), the contribution of the main ^{13}C−^{1}H dipolar interaction to the cumulative ^{13}C relaxation rate in Ala$^{\beta}$ $^{13}CHD_2$ methyls at 600 MHz spectrometer field is calculated to amount to only 81% with the remaining 19% arising from: (i) ^{13}C−^{2}H dipolar spin interactions including cross-correlated relaxation between the two ^{13}C−^{2}H dipoles,[38] 10%; (ii) methyl ^{13}C CSA, 5.5% if CSA = 18 ppm is assumed; and (iii) dipolar contributions from both ^{1}H and ^{2}H spins that are external to the methyl group in question contributing together 3.5%. The increased complexity of interpretation of ^{13}C relaxation data in terms of local dynamics parameters is, however, partially compensated by much higher sensitivity of the ^{13}C-based experiments. ^{13}C relaxation measurements in $^{13}CHD_2$ Ala$^{\beta}$ methyls of MSG are 4.5-fold(10-fold) more sensitive on average compared to their $R_2(R_1)$ ^{2}H counterparts. The $^{13}CHD_2$ labeling scheme employed for Ala$^{\beta}$ methyls in this study allows to measure both ^{2}H and ^{13}C relaxation rates within the same isotopomer (and the same protein sample),[38] and therefore to assess whether additional contributions to ^{13}C relaxation rates compromise the extraction of robust motional characteristics.

The ^{2}H $R_2[M_+(CHD_2)]$, $R_1[M_L(CHD_2)]$, and ^{13}C $R_{1\rho}$,R_1 rates measured at Ala$^{\beta}$ positions in {Ala$^{\beta}$-[$^{13}CHD_2$]}-labeled MSG are shown as a function of the protein sequence in Figures S1 and S2 of the Supporting Information. Figure S2 also shows ^{15}N $R_{1\rho}$ rates in MSG at 37 °C for comparison. Figure 2a shows the order parameter values (S^2_{axis}) of Ala$^{\beta}$ methyls derived from ^{2}H (red) and ^{13}C (black) relaxation data as a function of alanine residue numbers. A remarkably high level of agreement between ^{2}H-derived and ^{13}C-derived S^2_{axis} illustrated in Figure 2b (Pearson R = 0.976 for 59 peaks; pairwise rmsd between the sets of values of 0.036) makes it clear that Ala$^{\beta}$ ^{13}C relaxation rates generally serve as reliable measures of dynamics despite the increased complexity of data interpretation.

Whereas S^2_{axis} values of ILV methyls can be understood in terms of the rotameric preferences in methyl-containing side chains,[39,71,72] Ala$^{\beta}$ methyl groups practically constitute a part of the protein backbone and are significantly more ordered on average. Average ^{2}H(^{13}C)-derived S^2_{axis} values obtained in MSG are 0.90(0.89) after exclusion of the three flexible residues: Ala^{2} in the very N-terminus of the protein, Ala^{153} in the flexible loop of the α/β domain, and Ala^{585} in the flexible loop connecting the core of the molecule with the C-terminal plug (Figure 2a and Figures S1 and S2). Furthermore, except for the flexible loop (300−310) and two residues in the loop (614−631) flanking the active site, the flexibility of the backbone on the pico-to-nanosecond time scale is 'picked-up' by Ala$^{\beta}$ relaxation measurements in the same regions of the molecule as by ^{15}N R_{1p} data (Figure S2) emphasizing the utility of Ala$^{\beta}$ methyls as probes of backbone rather than side chain dynamics. Although ^{15}N−^{1}H amides are clearly more abundant probes of protein structure and dynamics (approximately 4 times more amide peaks can be completely resolved in the ^{15}N−^{1}H TROSY spectra than Ala$^{\beta}$ methyl peaks in methyl-TROSY spectra of MSG), the uniqueness of Ala$^{\beta}$ methyl probes derives from their proximity to the protein backbone on the one hand, and the favorable relaxation properties of the 3-fold degenerate $^{13}CH_3$ spin systems on the other hand. For example, the signal-to-noise of methyl peaks in methyl-TROSY spectra is on average 3-to-4-fold higher than that of amides in ^{15}N−^{1}H TROSY for the samples with approximately the same protein concentration. Therefore, it is rather the quality than the quantity of the probes that distinguishes Ala$^{\beta}$ methyls. As a result, more quantitative measurements of structural and dynamics NMR parameters are possible at Ala$^{\beta}$ sites.

As discussed on a number of occasions previously,[42] methyl τ_f values reflect in a complex way the combined time scales of

(71) Best, R. B.; Clarke, J.; Karplus, M. *J. Am. Chem. Soc.* **2004**, *126*, 7734.
(72) Best, R. B.; Rutherford, T. J.; Freund, S. M.; Clarke, J. *Biochemistry* **2004**, *43*, 1145.

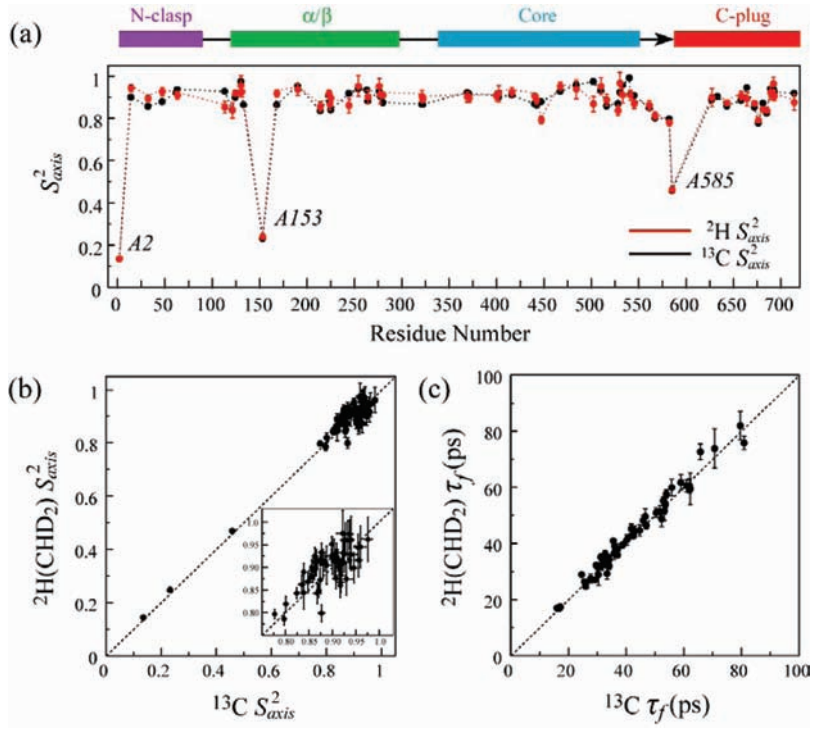

Figure 2. (a) ^{2}H-derived (red) and ^{13}C-derived (black) S^2_{axis} of Ala$^\beta$ methyls obtained in {Ala$^\beta$-[^{13}CHD$_2$]}-labeled MSG (37 °C) plotted as a function of alanine residue numbers. Positions of the four domains of MSG are schematically shown above the plot using the same color-coding as in Figure 1a. Location of the flexible loop connecting the core domain with the C-terminal plug (residues 550−588) is shown with an arrow. (b) A correlation plot comparing ^{2}H-derived (*y*-axis) and ^{13}C-derived (*x*-axis) Ala$^\beta$ methyl S^2_{axis}; linear regression of the data provides the slope of 0.973 ± 0.03 and the intercept 0.032 ± 0.02 (Pearson $R = 0.976$; 59 methyls). The inset shows a region of the correlation plot for $0.75 < S^2_{axis} < 1.05$. (c) A correlation plot comparing ^{2}H-derived (*y*-axis) and ^{13}C-derived (*x*-axis) correlation times of local motions (τ_f; ps) for 55 Ala$^\beta$ methyl groups. Linear regression of the data provided the slope of 0.997 and the intercept of 0.94 (Pearson $R = 0.988$). Ala^{130}, Ala^{263}, Ala^{484}, Ala^{540}, and Ala^{633} providing both ^{2}H- and ^{13}C-derived τ_f exceeding 100 ps have been excluded from the plot. The dashed lines in (b and c) correspond to $y = x$.

all motional processes that affect methyl R_1 relaxation including (fast) 3-fold methyl rotation.[73] Interestingly, five Ala$^\beta$ methyls (Ala^{130}, Ala^{263}, Ala^{484}, Ala^{540}, and Ala^{633}) provided τ_f values in excess of 100 ps (resulting from correspondingly elevated ^{13}C and ^{2}H R_1 rates; Figures S1b,d of the Supporting Information) indicating higher methyl rotation barriers and/or more complex dynamics of the Ala C$^\alpha$−C$^\beta$ axis at these positions. For example, the agreement between ^{13}C-derived and ^{2}H-derived τ_f values is poorer for the small subset of residues with τ_f in excess of 100 ps indicating that in these cases the spectral density of eq 1 may not give an adequate description of the motional processes experienced by the Ala C$^\alpha$−C$^\beta$ axis.[74] These 5 residues have been therefore excluded from the correlation plot of Figure 2c. Interestingly, two of these methyls (Ala^{130} and Ala^{633}) are located in close proximity to the glyoxylate and Acetyl-coA binding sites[35,36,39] (see discussion below). The distribution of τ_f values obtained in Ala$^\beta$ methyls is very similar to that obtained earlier for Leu$^\delta$ and Val$^\gamma$ methyls of MSG at the same temperature (37 °C), implying a similar barrier of methyl rotation in these side chains, ∼12 kJ/mol.[39,73]

^{13}C relaxation rates of several Ala$^\beta$ positions in MSG (Ala^{113}, Ala^{190}, Ala^{277}, Ala^{447}, Ala^{467}, Ala^{502}, and Ala^{533}) could not be interpreted using methyl ^{13}C CSA value of 18 ppm, consistently providing S^2_{axis} values close to or even higher than unity. According to solid-state NMR measurements, the chemical shielding tensor of Ala ^{13}C$^\beta$ is not axially symmetric (asymmetry $\eta = 1$)[75−77] and is more variable than that of ILV methyl carbons (±6 ppm[67]); the most shielded direction of the tensor is parallel to the C$^\alpha$−C$^\beta$ bond to within ±5°.[75] Introduction of asymmetry of the Ala$^\beta$ CSA tensor into the expression for CSA spectral density (eq 1; $a = 1$) cannot, however, fully account for the observed increase in ^{13}C R_2 rates of these methyls. Interestingly, the Ala$^\beta$ positions listed above are the most downfield-shifted in the ^{13}C dimension of ^{1}H−^{13}C correlation maps (see Figure 1c). These residues are highlighted in Figure 3a that shows the deviations of all Ala ^{13}C$^\beta$ shifts (Δ^{13}C$^\beta$) in MSG from the random coil value (19 ppm). Moreover, these Ala$^\beta$ positions (with the exception of Ala^{467} and Ala^{277}) are located at the leftmost upper corner of the Ramachandran map corresponding to fully extended conformation as shown in Figure 3b. A statistically significant correlation exists between (Δ^{13}C$^\beta$) and the value of φ angles for all nonhelical alanines of MSG (Figure 3c). It is conceivable that higher isotropic ^{13}C$^\beta$ shifts are accompanied by higher values of ^{13}C CSA, by analogy with the CSA of ^{13}C$^\alpha$ sites that has been shown to be highly variable and correlated with secondary structure.[78] Since residue-specific values of Ala ^{13}C$^\beta$ CSA in MSG are presently not available, we have set ^{13}C$^\beta$ CSA value for these seven alanines to 24 ppm, one standard deviation higher than the average. Using

(73) Xue, Y.; Pavlova, M. S.; Ryabov, Y. E.; Reif, B.; Skrynnikov, N. R. *J. Am. Chem. Soc.* **2007**, *129*, 6827.
(74) Showalter, S. A.; Johnson, E.; Rance, M.; Brüschweiler, R. *J. Am. Chem. Soc.* **2007**, *129*, 14146.
(75) Naito, A.; Ganapathy, S.; Akasaka, K.; McDowell, C. A. *J. Chem. Phys.* **1981**, *74*, 3190.
(76) Duma, L.; Hediger, S.; Lesage, A.; Sakellariou, D.; Emsley, L. *J. Magn. Reson.* **2003**, *162*, 90.
(77) Drobny, G. P.; Long, G. R.; Karlsson, T.; Shaw, W.; Popham, J.; Oyler, N.; Bower, P.; Stringer, J.; Gregory, D.; Mehta, M.; Stayton, P. S. *Annu. Rev. Phys. Chem.* **2003**, *54*, 531.
(78) Tjandra, N.; Bax, A. *J. Am. Chem. Soc.* **1997**, *119*, 9576.

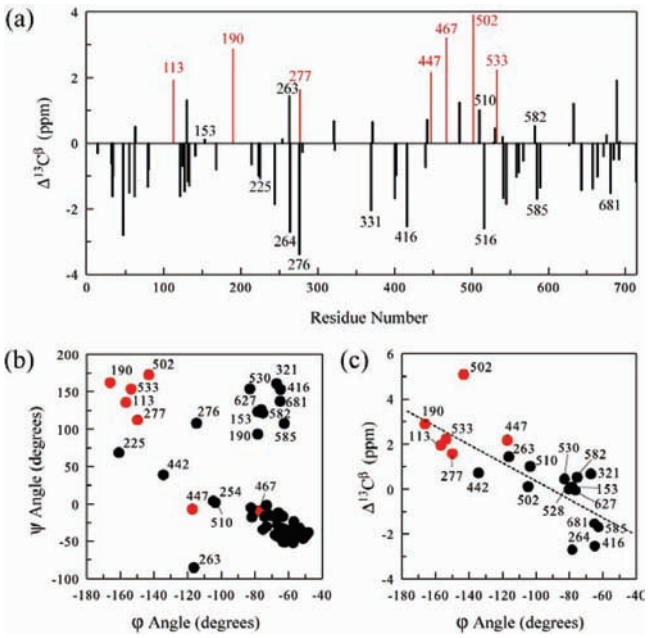

Figure 3. (a) Deviations of Ala $^{13}C^{\beta}$ chemical shifts of MSG from the random coil value ($\Delta^{13}C^{\beta}$) as a function of residue number. Alanine residues whose $^{13}C^{\beta}$ relaxation data could not be fitted with $^{13}C^{\beta}$ CSA = 18 ppm are shown in red. (b) A region of the Ramachandran map of alanines in MSG with the same residues shown with red circles. (c) A correlation plot of Ala $\Delta^{13}C^{\beta}$ (ppm) vs ϕ angles (Pearson $R = 0.79$; the angles have been calculated from the structure of MSG in complex with glyoxylate, pdb id code 1d8c.[35] Ala^{276} has been excluded from the plot as its C^{β} may experience significant ring-current shift from the adjacent indole ring of Trp^{610}.[29]

the S^2_{axis} and τ_f values from ^{2}H measurements and enforcing them in the analysis of ^{13}C relaxation rates for this subset of Ala$^{\beta}$ methyls provided ^{13}C chemical shift anisotropies (assuming axially symmetric CSA tensor) of 30, 26, 20, 31, 20, and 28 ppm for Ala^{113}, Ala^{190}, Ala^{277}, Ala^{447}, Ala^{467}, and Ala^{533}, respectively. The relaxation rates of Ala^{502} could be interpreted only assuming its $^{13}C^{\beta}$ CSA equal to or higher than 32 ppm, an anomalously high value for alanine methyl carbons.

Robust measures of methyl axis motions can be obtained also from ^{1}H relaxation measurements in $^{13}CH_3$ groups via relaxation-violated ('forbidden') coherence transfer NMR spectroscopy.[46] Such experiments quantify the build-up of methyl coherences arising from ^{1}H$-^1$H cross-correlated relaxation within A_3X spin-systems of $^{13}CH_3$ methyl groups attached to large macromolecules. The rates of ^{1}H$-^1$H cross-correlated relaxation (η) are direct measures of the amplitude of methyl axis motions (S^2_{axis}).[33,46] The 'forbidden' coherence transfer rates have been measured using the {Ala$^{\beta}$-[$^{13}CH_3$]; Ile$^{\delta 1}$-[$^{13}CH_3$]; Leu,Val-[$^{13}CH_3/^{12}CD_3$]}-labeled sample of MSG. Typical magnetization 'build-up' curves are shown in Figure S3a of the Supporting Information for several Ala$^{\beta}$ sites in MSG. Although a smaller subset of residues could be reliably quantified by 'forbidden' experiments even compared with the subset for which ^{2}H relaxation data from Ala$^{\beta}$-$^{13}CHD_2$ isotopomers is available, strong correlations of ^{1}H($^{13}CH_3$)-derived S^2_{axis} values with their ^{2}H-derived counterparts are observed (Figure S3b of the Supporting Information; Pearson $R = 0.979$ for 50 sites).

Dynamics of Ala$^{\beta}$ Methyls in MSG on the Micro-to-Millisecond Time Scale. The methyl-TROSY-based relaxation dispersion experiment[45] performed on {Ala$^{\beta}$-[$^{13}CH_3$]; Ile$^{\delta 1}$-[$^{13}CH_3$]; Leu,Val-[$^{13}CH_3/^{12}CD_3$]}-MSG yielded only three Ala$^{\beta}$ methyls with exchange contribution $R_{ex} > 2$ s^{-1} and dispersion profiles that could be quantified with confidence. MQ relaxation dispersion profiles of the three methyls (Ala^{402}, Ala^{510}, and Ala^{627}) are shown in Figure 4a. C^{β} atoms of the two of these methyls [Ala^{510} ($k_{ex} = 861 \pm 5$ s^{-1}; $\Delta\omega_C = 0.36$ ppm; $\Delta\omega_H = 0$ ppm) and Ala^{627} ($k_{ex} = 781 \pm 16$ s^{-1}; $\Delta\omega_C = 0.30$ ppm; $\Delta\omega_H = 0.02$ ppm)] are located in relative proximity to the pyruvate-Acetyl-CoA binding site in the X-ray structure of the ternary abortive MSG−pyruvate−acetyl-CoA complex,[36] within 7 Å from the carbon atoms of the pantothenate moiety of Acetyl-CoA. The methyl group of another alanine, Ala^{633}, that 'overhangs' the pyruvate/glyoxylate binding site, provided very weak correlations in all experiments and could not be quantified in MQ CPMG measurements. It is, however, noticeably exchange-broadened in the ^{1}H dimension of 2D ^{1}H$-^{13}$C correlation maps. Furthermore, Ala^{633} is also the only residue in the protein whose $^{13}C^{\beta}$ $R_{1\rho}$ relaxation rate showed substantial reduction (4 s^{-1}) upon increase of the strength of ^{13}C spin-lock field from 1.2 to 2.0 kHz (see Materials and Methods) indicating that exchange processes at this methyl position are not completely quenched by the spin-lock fields employed in ^{13}C $R_{1\rho}$ measurements.

Figure 4b highlights C^{β} positions of Ala^{633}, Ala^{510}, and Ala^{627} on the X-ray structure of the MSG−pyruvate−acetyl-CoA complex.[36] Previous quantitative ^{2}H and ^{13}C relaxation studies of ILV side chain dynamics in MSG complexes revealed a binding interface that is dynamic on multiple time scales and that at least partially rigidifies upon binding of pyruvate and Acetyl-CoA to the apo-form of the enzyme.[39] In agreement with these earlier observations, Ala^{633} and Ala^{627} located in the same loop of the C-terminal plug of MSG (residues 614−631), and Ala^{510} in a loop of the molecular core (residues 506−515)—both loops flanking the binding sites of glyoxylate/pyruvate and Acetyl-CoA, respectively—are flexible on the micro-to-millisecond time scale in the apo-form of the enzyme studied here.

Probing Molecular Structure of MSG by Ala$^{\beta}$ Methyl ^{1}H$-^{13}$C Residual Dipolar Couplings. Methyl ^{1}H$-^{13}$C residual dipolar couplings (RDCs) can be measured in selectively $^{13}CH_3$-methyl-labeled large proteins using the IPAP[47,48] principle in the acquisition dimension (F_2) of 2D methyl-TROSY spectra.[79] In our hands, more accurate results are obtained if ^{1}H$-^{13}$C methyl RDCs ($^1D_{CH}$) are measured in the indirect (F_1) dimension of the 2D spectra recorded on methyl groups of $^{13}CHD_2$ variety. The utility of $^{13}CHD_2$ methyl isotopomers has been very recently demonstrated on a number of occasions in applications to very large molecular assemblies by Kay and co-workers.[84,85]

Figure 5 shows the gradient sensitivity-enhanced[81,82] pulse-scheme used for the measurement of $^1D_{CH}$ couplings in {Ala$^{\beta}$-[$^{13}CHD_2$]}-labeled MSG. The pulse-scheme is very similar to the recently reported experiment for accurate measurement of ^{1}H$-^{15}$N RDCs in protonated proteins.[86] Briefly, two experiments are performed: (i) one with the ^{1}H pulses shown with open rectangles in Figure 5 applied at positions *a* resulting in the

(79) Sprangers, R.; Kay, L. E. *J. Am. Chem. Soc.* **2007**, *24*, 12668.
(80) Shaka, A. J.; Keeler, J.; Frenkiel, T.; Freeman, R. *J. Magn. Reson.* **1983**, *52*, 335.
(81) Kay, L. E.; Keifer, P.; Saarinen, T. *J. Am. Chem. Soc.* **1992**, *114*, 10663.
(82) Schleucher, J.; Sattler, M.; Griesinger, C. *Angew. Chem., Int. Ed. Engl.* **1993**, *32*, 1489.
(83) Marion, D.; Ikura, M.; Tschudin, R.; Bax, A. *J. Magn. Reson.* **1989**, *85*, 393.
(84) Religa, T. L.; Kay, L. E. *J. Biomol. NMR* **2010**, *47*, 163.
(85) Baldwin, A. J.; Religa, T. L.; Hansen, D. F.; Bouvignies, G.; Kay, L. E. *J. Am. Chem. Soc.* **2010**, *132*, 10992.
(86) Yao, L. Y. J.; Bax, A. *J. Biomol. NMR* **2009**, *43*, 161.

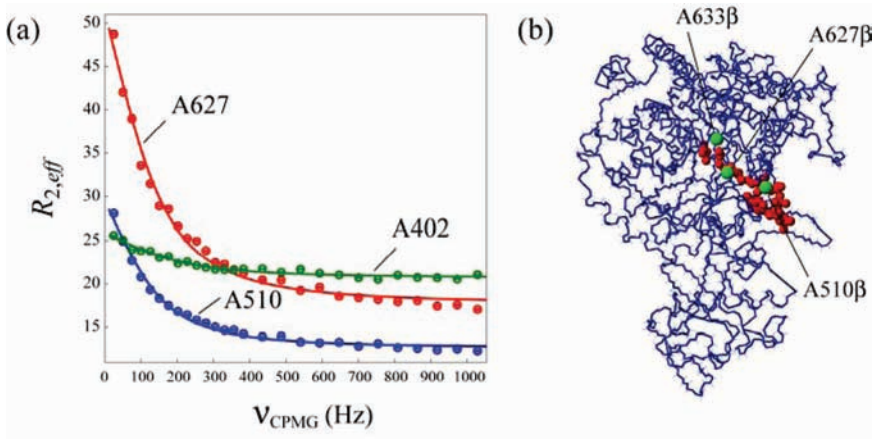

Figure 4. (a) Relaxation dispersion curves for the three Ala$^{\beta}$ methyls of MSG with $R_{ex} > 2$ s^{-1} obtained in {Ala$^{\beta}$-[^{13}CH$_3$]; Ile$^{\delta 1}$-[^{13}CH$_3$]; Leu,Val-[^{13}CH$_3$/^{12}CD$_3$]}-labeled MSG (37 °C; 600 MHz). (b) Schematic representation of the crystal structure of MSG (blue) in the ternary abortive complex with pyruvate and Acetyl-CoA (both shown with red spheres; pdb id code 1p7t[36]). The three alanine methyls dynamic on the micro-to-millisecond time scale (Ala^{633}, Ala^{510}, Ala^{627}) in the vicinity of the pyruvate-Acetyl-CoA binding site are shown with green spheres.

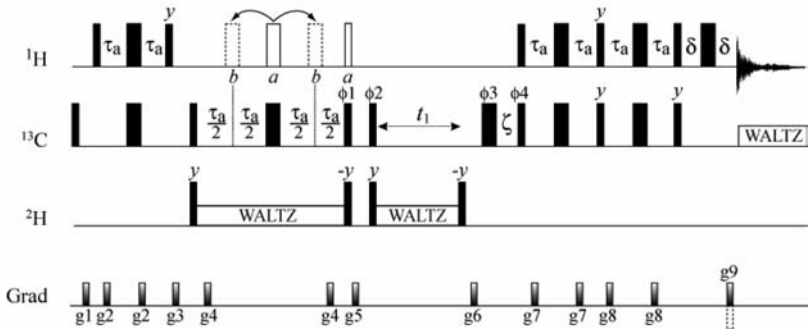

Figure 5. The IPAP-HSQC scheme for the measurement of methyl $^1D_{CH}$ residual dipolar couplings in $^{13}CHD_2$-methyl-labeled large proteins. All narrow(wide) rectangular pulses are applied with flip angles of 90°(180°) along the *x*-axis unless indicated otherwise. The pulses shown with open rectangles at points *a* are applied for the measurements that yield AP subspectra. For the measurement of IP subspectra, the pulses shown with dashed rectangles at points *b* are applied instead. ^{13}C Waltz-16[80] decoupling is achieved using a 2-kHz field, while ^{2}H Waltz-16[80] decoupling uses a 0.9 kHz field. The ^{1}H and ^{2}H carriers are positioned at 1.5 ppm. The ^{13}C carrier is placed at 19 ppm. The recovery delay was set to 2.2 s. Delays are: $\tau_a = 2.0$ ms; $\delta = 400$ μs; delay ζ should be equal to the length of gradient g6 plus the associated gradient recovery delay. The phase-cycle is: $\phi 1 = x$ for IP spectra and $\phi 1 = y$ for the AP spectra; $\phi 2 = x,-x$; $\phi 3 = x,-x,y,-y$; $\phi 4 = x$; receiver $= x,-x,-x,x$. Quadrature detection in the F_1 dimension is achieved by an increment of the phase $\phi 4$ and inversion of the sign of gradient g9.[81,82] $\phi 2$ is increased by 180° for each t_1 point.[83] Durations and strengths of the pulsed-field gradients in units of (ms; Gauss/cm) are: g1 = (1.0; 10), g2 = (0.3; 8), g3 = (1.0; 12), g4 = (0.5; 10), g5 = (1.0; 10), g6 = (1.0; 15), g7 = (0.4; 12), g8 = (0.4; 8), g9 = (0.254; 15).

anti-phase (AP) doublets in the ^{13}C(F_1) dimension of the spectrum, and (ii) the second experiment with the 180° ^{1}H pulses shown with dashed rectangles applied at positions *b* (Figure 5) resulting in the in-phase (IP) doublets in F_1. Addition (IP + AP) and subtraction (IP − AP) of the two data sets lead to separation of the two ^{1}H−^{13}C doublet components. Figure 6b(c) shows the superposition of the two components of the doublet in the isotropic(aligned) phase from a selected region of the ^{1}H/^{2}H-F_1-decoupled 2D gradient sensitivity-enhanced ^{1}H−^{13}C HSQC[81,87,88] correlation map of {Ala$^{\beta}$-[^{13}CHD$_2$]}-MSG highlighted in Figure 6a. $^1D_{CH}$ couplings in the range between −16 and +21 Hz have been obtained in pf1 phage-aligned[49] MSG. Pair-wise rmsd of the $^1D_{CH}$ couplings obtained from duplicate measurements was 0.55 Hz indicating the error in the measurement of 0.4 Hz. In fact, using the experiment of Figure 5, it was possible to pinpoint the small difference between the isotropic scalar coupling values ($^1J_{CH}$) in Ala$^{\beta}$-[^{13}CHD$_2$] (129.3 ± 0.7 Hz on average) and Ala$^{\beta}$-[^{13}CH$_3$] (130.0 ± 0.7 Hz on average) samples of MSG in full agreement with the difference between the two methyl isotopomers noted earlier.[63]

Using the parameters of the alignment tensor[89] established for MSG previously under the same experimental conditions[32] ($A_a = -1.6 \times 10^{-3}$; $R = 0.4$; $\alpha = 7°$; $\beta = 133°$; $\gamma = 243°$ where A_a and R are axial and rhombic components of the alignment tensor and the Euler angles {α; β; γ} describe the orientation of the principal axes with respect to the PDB frame of MSG), we concentrated on the subset of Ala$^{\beta}$ methyls with $S_{axis} > 0.9$ and $^1D_{CH}$ couplings reproducible to within 2 uncertainties in the measurement. Figure 6d shows the correlation between experimental $^1D_{CH}$ couplings obtained for Ala$^{\beta}$ methyls in apo-MSG and those calculated from the X-ray structure of MSG in complex with glyoxylate.[35] The *Q* factor[90] of the correlation is 0.31 (Pearson $R = 0.953$ for 47 peaks). Very similar correlation is obtained when the coordinates of the MSG in complex with pyruvate and Acetyl-CoA are used.[36] Four alanine residues (Ala^{280}, Ala^{510}, Ala^{633}, and Ala^{685}) have the largest discrepancies between the experimentally measured and calculated $^1D_{CH}$ couplings (shown with red circles in Figure 6d). As noted above, Ala^{510} and Ala^{633} are located in the vicinity of the binding site and are likely to have different conformations in the ligand-free form of MSG studied here. Ala^{685} belongs to

(87) Bodenhausen, G.; Rubin, D. J. *Chem. Phys. Lett.* **1980**, *69*, 185.
(88) Palmer, A. G.; Cavanagh, J.; Wright, P. E.; Rance, M. *J. Magn. Reson.* **1991**, *93*, 151.
(89) Tjandra, N.; Bax, A. *Science* **1997**, *278*, 1111.
(90) Ottiger, M.; Bax, A. *J. Biomol. NMR* **1999**, *13*, 187.

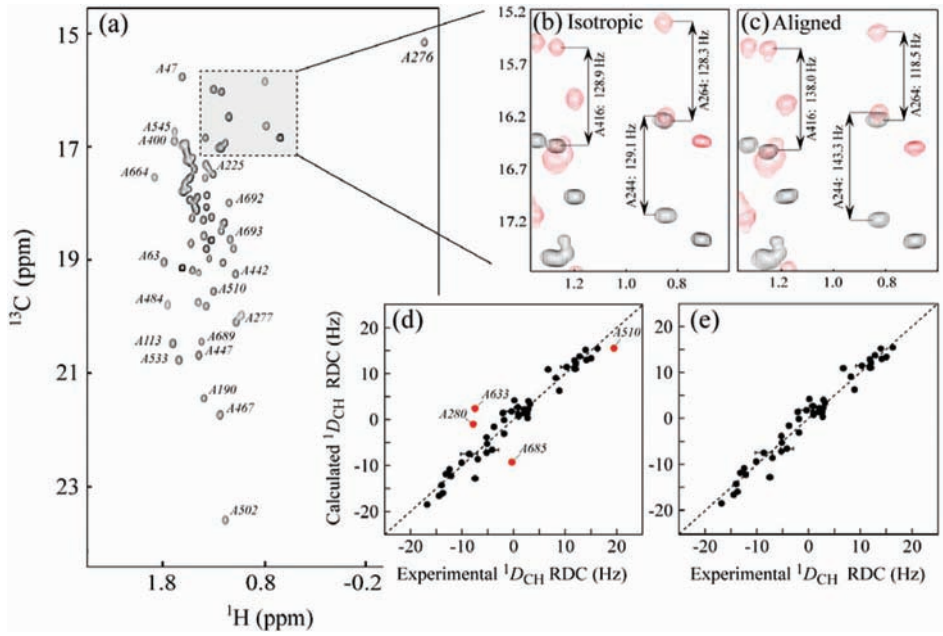

Figure 6. (a) 2D HSQC correlation map recorded on the {Ala$^{\beta}$-[^{13}CHD$_2$]}-labeled MSG (37 °C; 600 MHz). Selected assignments of Ala$^{\beta}$ resonances are labeled with residue numbers. (b and c) A superposition of a selected region of the 2D IP + AP (red) and IP − AP (black) spectra recorded on MSG in (b) isotropic, and (c) aligned phase. The sample of MSG was oriented in pf1 phage (∼12 mg/mL; D_2O splitting 10 Hz). (d and e) Correlation plots comparing experimental and calculated methyl $^{1}D_{CH}$ RDCs obtained from {Ala$^{\beta}$-[^{13}CHD$_2$]}-MSG. The four residues with the largest discrepancies between experimental and calculated values are shown with red circles in (d) and eliminated in (e). Pearson $R = 0.953(0.981)$ for the plots in d(e). Linear regression of the data provided the slope of $0.97 \pm 0.05(1.02 \pm 0.03)$ and the intercept of $0.11 \pm 0.43(0.03 \pm 0.29)$ in the plots d(e). Dashed lines correspond to $y = x$.

a loop in the C-terminal domain whose conformation may also experience minor differences in the different ligation states of the enzyme. Despite the fact that no significant reorientation of the C-terminal domain occurs in MSG upon formation of complexes with its substrates as established earlier from analysis of backbone ^{15}N−^{1}HN RDCs and anisotropic ^{13}CO shifts,[32] significant variation in orientation of certain C$^{\alpha}$−C$^{\beta}$ bond vectors can be envisaged. Upon elimination of these four residues, the *Q* factor reduces to 0.21 (Figure 6e; Pearson $R = 0.981$). Of note, the order parameter S_{axis} that is commonly necessary for interpretation of methyl $^{1}D_{CH}$ couplings of ILV methyls can be set to a uniform value of 0.95 for Ala$^{\beta}$ $^{1}D_{CH}$ RDCs, much in the same manner as is usually used for interpretation of backbone ^{1}H−^{15}N dipolar couplings in proteins.

Ala$^{\beta}$-ILV Methyl-TROSY NOE Spectroscopy. Proximity to the protein backbone and a high degree of order makes Ala$^{\beta}$ methyl groups especially useful probes for determination of NOE contacts within large protein structures. Earlier, 4D methyl-TROSY spectroscopy was used in conjunction with nonuniform data sampling and multidimensional decomposition (MDD)[52] to resolve as many ILV methyl−methyl NOE contacts in MSG as possible. Here, in view of a limited set of additional (Ala) probes, we used 3D methyl-TROSY NOE spectroscopy and uniform sampling for detecting NOEs within the Ala$^{\beta}$ group (Ala$^{\beta}$−Ala$^{\beta}$) as well as between Ala$^{\beta}$ and ILV methyl groups (Ala$^{\beta}$-ILV).

The pulse schemes for the 3D methyl ^{1}H−^{13}C HMQC-NOESY (HHC-NOESY) and 3D methyl ^{1}H−^{13}C HMQC-NOESY-HMQC (HCC-NOESY) experiments used for assignments of NOE contacts in {Ala$^{\beta}$-[^{13}CH$_3$]; Ile$^{\delta1}$-[^{13}CH$_3$]; Leu, Val-[^{13}CH$_3$/^{12}CD$_3$]}-MSG are shown in Figure S4 of the Supporting Information. These experiments preserve methyl magnetization in the MQ state during both ^{1}H and ^{13}C indirect evolution periods and are straightforward adaptations of the methyl-TROSY 4D HMQC-NOESY-HMQC scheme[52] used for assignments of ILV NOEs in MSG previously. The HHC-NOESY pulse scheme of Figure S4a is especially sensitive as the acquisition of the signal is performed immediately after the NOE mixing period keeping the number of ^{1}H−^{13}C magnetization transfer steps to a minimum. Even though the resolving power of 4D spectroscopy in such methyl-abundant large proteins as MSG is unsurpassable, the information content of the 4D spectra can be retrieved from the 3D data sets if the symmetry of NOE cross-peaks is used effectively. Below we briefly describe how the symmetric properties of the two acquired 3D NOE data sets can be utilized for assignments of methyl−methyl NOE cross-peaks.

Figure 7a shows a plane from the 3D ^{1}H−^{13}C HHC-NOESY experiments drawn at the F_1(^{13}C) chemical shift of the 'origin' methyl group of Ala^{63} (19.4 ppm). A number of NOE cross-peaks originating from Ala^{63} are labeled with methyl assignments in Figure 7a. The chemical shifts of 'destination' methyl protons are to be taken from the F_3(^{1}H) (directly detected) dimension. As it is shown in Figure 7b, in the plane from the HCC-NOESY spectrum corresponding to the same F_1(^{13}C) chemical shift of the 'origin' Ala^{63} methyl (19.4 ppm), the F_3(^{1}H) chemical shift of one of the correlations (labeled with 'Leu$^{88\delta2}$' in Figure 7a) corresponds to a correlation with the ^{13}C(F_2) chemical shift of the 'destination' methyl group (25.4 ppm; Figure 7b). Identification of a plane from the 3D HHC-NOESY data set corresponding to the F_1(^{13}C) chemical shift of this 'destination' methyl ^{13}C shift (25.4 ppm) provides the 'symmetry correlation' at the F_3(^{1}H) chemical shift of the 'origin' Ala^{63} (Figure 7c; the 'symmetry correlation' is labeled with a red asterisk). This identification is confirmed by an existing correlation at this pair of [^{1}H,^{13}C] chemical shifts in the 2D ^{1}H−^{13}C HMQC correlation map shown in Figure 7d. Frequently, many NOE correlations may exist along the F_2(^{13}C) dimension of the HCC-NOESY data set that have the same (or very similar) F_3(^{1}H) chemical shifts. Then, each of the possibilities should

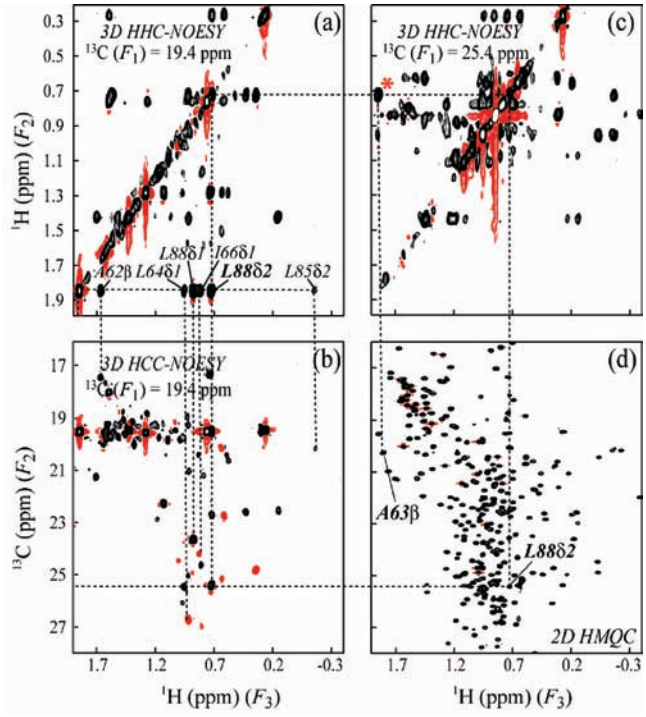

Figure 7. Selected planes from the 3D methyl ^{1}H−^{13}C HMQC-NOESY (HHC-NOESY) spectrum and 3D methyl ^{1}H−^{13}C HMQC-NOESY-HMQC (HCC-NOESY) experiments used for assignments of NOE contacts in {Ala$^{\beta}$-[^{13}CH$_3$]; Ile$^{\delta 1}$-[^{13}CH$_3$]; Leu,Val-[^{13}CH$_3$/^{12}CD$_3$]}-MSG. Negative contours are shown in red. (a) A plane from the HHC-NOESY spectrum corresponding to the F_1(^{13}C) chemical shift of the 'origin' methyl group of Ala^{63} (19.4 ppm). (b) A plane from the HCC-NOESY spectrum corresponding to the same F_1(^{13}C) chemical shift as in (a), 'origin' methyl of Ala^{63} (19.4 ppm). (c) A plane from the HHC-NOESY spectrum corresponding to the F_1(^{13}C) chemical shift of the 'destination' δ2 methyl group of Leu7^{88} (25.4 ppm). The 'symmetry correlation' Leu$^{88\delta 2}$−Ala$^{63\beta}$ is marked with a red asterisk. (d) A region of the 2D methyl ^{1}H−^{13}C HMQC spectrum of {Ala$^{\beta}$-[^{13}CH$_3$]; Ile$^{\delta 1}$-[^{13}CH$_3$]; Leu,Val-[^{13}CH$_3$/^{12}CD$_3$]}-MSG. Cross-peak positions of the 'origin' methyl of Ala^{63} and 'destination' methyl of Leu^{88} are labeled in bold.

be explored by inspection of the planes of the HHC-NOESY spectrum (Figure 7c) corresponding to each putative 'destination' methyl chemical shift (F_1,^{13}C). The number of such possibilities is, however, reduced by inspection of the 2D ^{1}H−^{13}C HMQC correlation map (Figure 7d) in search of existing correlations at the corresponding pair of [^{1}H,^{13}C] chemical shifts.

A total of 152 Ala$^{\beta}$-ILV and Ala$^{\beta}$−Ala$^{\beta}$ methyl−methyl NOE contacts could be assigned from the two 3D NOESY data described above. This includes 118 long-range (between residue i and residue j; $|i-j| > 3$) and 34 short-range ($|i-j| \leq 3$) contacts. Among these 20 NOE contacts have been assigned for which $|i-j| = 3$. The vast majority of these NOE contacts are between Ala$^{\beta}$ and ILV methyl groups, with only 6(10) long-range(short-range) Ala$^{\beta}$−Ala$^{\beta}$ NOEs identified from the 3D spectra. Figure 8 shows a histogram of the fraction of the total number of identified NOEs (gray bars) and long-range NOEs (black bars) involving Ala$^{\beta}$ methyl groups as a function of the methyl−methyl distance ranges. Although above 5 Å the fraction of observed NOE contacts is below 50% of those calculated from the X-ray structure of MSG, the contacts between several methyl protons separated by a distance of up to 9 to 10 Å can be observed in very favorable cases. Although the number of unambiguously identified NOEs involving Ala methyl groups in this work is relatively small—if only long-range ($|i-j| > 3$) interactions are considered, the addition of new NOE contacts amounts to only

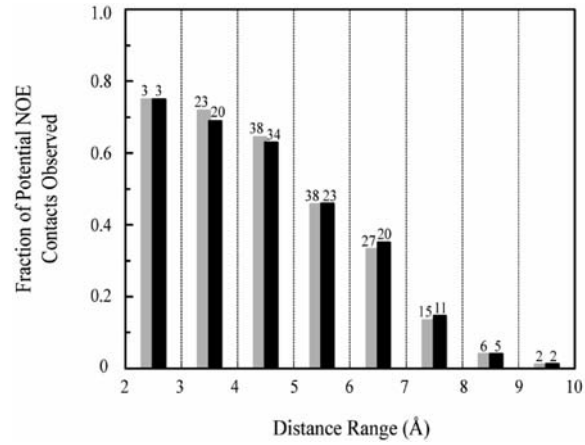

Figure 8. A histogram showing the fraction of the total number of observable NOEs (gray bars) and long-range ($|i-j| > 3$) NOEs (black bars) involving Ala$^{\beta}$ methyl groups as a function of the methyl−methyl distance ranges in MSG. Methyl−methyl distances have been calculated between geometric centers of the three proton positions in a methyl group. The total number of observed NOE contacts is indicated on top of each bar.

19% of the previously identified long-range interactions[10]—NOE contacts involving Ala$^{\beta}$ methyls may be expected to be more amenable to quantitative interpretation for derivation of accurate distance restraints in large proteins.[91]

Concluding Remarks

In summary, we characterized the utility of Ala$^{\beta}$ methyl groups as NMR probes of molecular structure and dynamics in high-molecular-weight proteins. First, using ^{2}H and ^{13}C relaxation measurements in {U-^{2}H; Ala$^{\beta}$-[^{13}CHD$_2$]}-labeled MSG, we showed that the vast majority of selectively labeled Ala$^{\beta}$ methyl groups are highly ordered with only a few exceptions. Proximity of Ala$^{\beta}$ methyls to the protein backbone and their high degree of ordering turn them into especially useful targets for a number of NMR applications that probe structure and dynamics of large protein molecules: (i) the measurement of methyl ^{1}H−^{13}C residual dipolar couplings, (ii) characterization of slow (μs-to-ms) dynamics at ligand binding interfaces, as well as (iii) methyl-TROSY-based NOE spectroscopy performed on {Ala$^{\beta}$-[^{13}CH$_3$]; Ile$^{\delta 1}$-[^{13}CH$_3$]; Leu,Val-[^{13}CH$_3$/^{12}CD$_3$]}-labeled samples where the number of methyl probes for derivation of distance restraints is increased compared to the state-of-the-art ILV labeling methodology. Even though the number of additional distance restraints (from NOE spectroscopy) and global bond-vector restraints (from RDC measurements) that could be derived from Ala$^{\beta}$ methyl probes in MSG is relatively small and evidently does not warrant attempts at refinement of the NMR-derived global backbone fold,[10,37] the present work will be of use as a benchmark study for biomolecular NMR spectroscopists, structural biologists, and biophysical chemists who contemplate application of selective methyl labeling methodologies for solution studies of large proteins and protein−protein complexes.

Acknowledgment. This work was supported by the Nano-Biotechnology Award to V.T. from the University of Maryland.

(91) Sounier, R.; Blanchard, L.; Wu, Z.; Boisbouvier, J. *J. Am. Chem. Soc.* **2007**, *129*, 472.

The authors thank Dr. C. T. Tan (Isotec/Sigma-Aldrich, Miamisburg, OH) for the synthesis of {3,3-d_2,3-$^{13}C_1$}-L-alanine.

Supporting Information Available: Figure S1 showing ^{2}H $R_2[M_+(CHD_2)]$, $R_1[M_L(CHD_2)]$, and ^{13}C R_2, R_1 relaxation rates measured at Ala$^\beta$ positions of {Ala$^\beta$-[$^{13}CHD_2$]}-MSG as a function of the protein sequence. Figure S2 comparing residue-specific ^{2}H $R_2[M_+(CHD_2)]$, ^{13}C R_2 and backbone amide ^{15}N R_2 rates of MSG. Figure S3 showing the build-up curves of 'forbidden' magnetization for several Ala$^\beta$ sites in MSG; also shown is a correlation plot of $^1H(^{13}CH_3)$-derived S^2_{axis} values vs ^{2}H-derived S^2_{axis}. Figure S4 showing ^{1}H−^{13}C 3D HMQC-NOESY and 3D HMQC-NOESY-HMQC pulse-schemes used in this work for collection of Ala$^\beta$-ILV and Ala$^\beta$−Ala$^\beta$ NOEs. This material is available free of charge via the Internet at http://pubs.acs.org.

JA1083656